energies

MDPI

Article

Forced Convection of Pulsating Nanofluid Flow over a Backward Facing Step with Various Particle Shapes

Ali J. Chamkha [1,2] and Fatih Selimefendigil [3,*]

[1] Mechanical Engineering Department, Prince Sultan Endowment for Energy and Environment, Prince Mohammad Bin Fahd University, Al-Khobar 31952, Saudi Arabia; achamkha@pmu.edu.sa or achamkha@yahoo.com

[2] RAK Research and Innovation Center, American University of Ras Al Khaimah, Ras Al-Khaimah P.O. Box 10021, UAE

[3] Department of Mechanical Engineering, Celal Bayar University, Manisa 45140, Turkey

* Correspondence: fthsel@yahoo.com; Tel.: +90-2236-2012370

Received: 15 October 2018; Accepted: 5 November 2018; Published: 7 November 2018

Abstract: In this study, numerical analysis of forced convective pulsating nanofluid flow over a backward-facing step with different nanoparticle shapes was performed by the finite volume method. The effects of the Strouhal number (between 0.1 and 2), solid nanoparticle volume fraction (between 0 and 0.04) and nanoparticle shapes (spherical, blade and cylindrical) on the heat transfer and fluid flow were examined with the aid of numerical simulation. It was observed that the average Nusselt number is a decreasing function of the Strouhal number for the considered range, and it enhances for higher solid particle fractions. Using nanofluids with spherical particles is advantageous in pulsating flow, whereas cylindrically-shaped particles are preferred in steady flow configurations. Average Nusselt number enhancements up to 30.24% and 27.95% are achieved with cylindrical- and spherical-shaped particles at the highest volume fraction.

Keywords: backward-facing step; pulsating flow; nanofluid; finite volume method

1. Introduction

In a wide range of engineering applications, flow separation and subsequent reattachment play an important role such as in cooling of electronic devices, flow around buildings, solar collectors, combustion chambers and many other systems. The flow over a backward-facing step geometry is a benchmark problem where this phenomena occurs. A vast amount of numerical and experimental research studies related to fluid flow and heat transfer over a backward-facing step can be found in various references. In the experimental study of [1], laminar flow over a backward-facing step in a two-dimensional configuration was studied by measuring the reattachment length and velocity distribution. Their results indicated that different flow regimes can be identified by the variation of the separation length. In the experimental work of [2], flow over a forward-facing step was analyzed, and the mechanisms that played an important role in the reattachment length were highlighted. A comprehensive review study for mixed convection of laminar flow over inclined step geometries was given in [3], which revealed the influence of various pertinent parameters such as the Reynolds number, Prandtl number and expansion ratio on the convective heat transfer features. A linear stability analysis of the fluid flow over a backward-facing step geometry for Reynolds numbers between 450 and 1050 was performed in [4]. In the numerical work of Iwai et al. [5], convective heat transfer over a backward-facing step geometry in a three-dimensional configuration for a low Reynolds number with various values of aspect ratios was shown. They observed that the maximum Nusselt number appeared near the two side walls. There were also studies that used different strategies such as a stationary cylinder [6] or a rotating cylinder [7], the flexibility of the wall [8] and a magnetic field [9] to affect

the flow separation characteristics and convective flow features for flow over the backward-facing step geometry.

Flow pulsation can be utilized to affect the flow field and heat transfer characteristics. An experimental study of pulsating flow for convection in a grooved channel was performed by Jin et al. [10]. It was observed that heat transfer enhances due to the vortex generation from the groove to the main stream with the flow pulsation. In the study by Faghri et al. [11], it was observed that additional terms appeared in the energy equation due to the interaction of velocity and temperature oscillations, and thus, the heat transfer rate was found to be affected. In the numerical study of [12], the hydro-thermal performance features of a pipe in pulsating flow conditions was examined. The effects of pulsation were found to be significant in a thin layer near the solid walls for higher frequencies, while the pulsation amplitude enhanced the heat transfer rate. In the analytical study of Nield and Kuznetsov [13], the perturbation technique was used to analyze the forced convection in a channel with a fluctuating pressure gradient. The magnitude and phase of the Nusselt number were changed for higher values of a dimensionless frequency.

Recently, nanofluids have been increasingly used in different heat transfer engineering problems. Nano-sized metallic or non-metallic particles such as Cu, Au, Al_2O_3, SiO_2, TiO_2 and CuO were used in the heat transfer fluid for various solid volume fractions. The average size of the particles was less than 100 nm. The higher conductivity of nanoparticles even at low particle concentration results in higher thermal conductivity of the base fluid and improves the thermal characteristics of the system. Nanoparticle size, type and shape are important factors for the thermal conductivity enhancement of the nanofluid with nanoparticles. Convective flow over a backward-facing step with nanofluids was performed by Abu-Nada [14]. It was reported that a better heat transfer characteristic was obtained in the recirculation zone for nanoparticles with lower thermal conductivity, and a higher nanoparticles solid volume fraction resulted in higher values of average heat transfer. Turbulent flow over a double forward-facing step was numerically examined for two different nanoparticle types in the study by Togun et al. [15]. Selimefendigil and Oztop [16] performed a numerical study of pulsating nanofluid flow over a backward-facing step and showed that the frequency of the pulsation and nanoparticle volume fraction enhanced the average heat transfer. In the literature, there are a few studies investigating the effects of nanoparticle shape on the convective heat transfer characteristics in various thermal engineering applications [17–19]. Vanaki et al. [19] performed a numerical study for the convective heat transfer in a wavy channel with different SiO_2 nanoparticle shapes with ethylene glycol. The platelet nanoparticle shape was found to have the best heat transfer performance. In the study by [20], the shape of the particle was observed to play an important role in the enhancement of the thermal conductivity of ZnO-water nanofluid. Murshed et al. [21] showed that the particle size and shape have significant effects on the thermal conductivity enhancement of TiO_2-water nanofluid.

To the best of our knowledge, laminar convection of pulsating flow over a backward-facing step with nanofluids and different nanoparticle shapes has never been investigated before. The flow pulsation and change of the thermo-physical properties of heat transfer fluid with different nanoparticle shapes for a backward-facing step geometry have the potential to improve the thermal characteristics of a thermal engineering system where flow separation and reattachment occur. Compact, energy-efficient and lightweight solutions for thermal engineering systems can be obtained. The results of this numerical study could be utilized in the thermal design and optimization of various systems, as mentioned above.

2. Mathematical Formulation

A schematic description of the backward-facing step geometry is depicted in Figure 1. The channel expansion ratio is two, and the step size is H. The length of the channel is $50H$, and the size of the downstream part starting from the edge of the step is $35H$. At the inlet of the channel, a parabolic velocity with an average value of u_0 is imposed. The velocity has a time- dependent part with an amplitude of A and a frequency of f. The downstream part of the channel from the edge of the step until

the exit is kept at a constant temperature of T_h, while at the inlet of the channel, fluid is at a temperature of T_c with $T_h > T_c$. The channel is filled with SiO_2 nanofluid of different particle types (spherical, blade, cylindrical). Unsteady, laminar, two-dimensional flow was assumed. Thermal radiation and viscous dissipation effects were neglected. The effect of natural convection was negligible. Flow pulsation amplitude was fixed to $A = 0.6$. It is expected for different nanoparticle volume fractions and shapes of nanoparticles that the fluid flow and heat transfer characteristics will be affected for the backward-facing step geometry in pulsating flow conditions. The thermo-physical properties of water and SiO_2 nanoparticles at temperature of 300 K are presented in Table 1 [19].

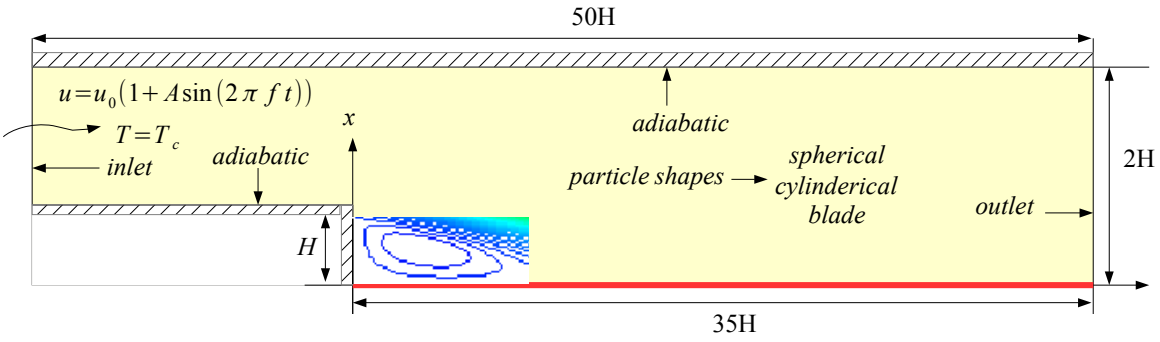

Figure 1. Schematic description of the backward-facing step geometry with boundary conditions.

Table 1. Thermophysical properties of the base fluid and the SiO_2 nanoparticle [19].

Property	Water	SiO_2
ρ (kg/m^3)	998.2	2200
c_p (J/kg K)	4812	703
k (W/mK)	0.61	1.2
μ (N s/m^2)	0.001003	-

Conservation equations for fluid flow and heat transfer in the dimensional form for a two-dimensional Cartesian coordinate system are stated as follows:

$$\frac{\partial u}{\partial x} + \frac{\partial v}{\partial y} = 0 \tag{1}$$

$$\frac{\partial u}{\partial t} + u\frac{\partial u}{\partial x} + v\frac{\partial u}{\partial y} = -\frac{1}{\rho_{nf}}\frac{\partial p}{\partial x} + \nu_{nf}\left(\frac{\partial^2 u}{\partial x^2} + \frac{\partial^2 u}{\partial y^2}\right) \tag{2}$$

$$\frac{\partial v}{\partial t} + u\frac{\partial v}{\partial x} + v\frac{\partial v}{\partial y} = -\frac{1}{\rho_{nf}}\frac{\partial p}{\partial y} + \nu_{nf}\left(\frac{\partial^2 v}{\partial x^2} + \frac{\partial^2 v}{\partial y^2}\right) \tag{3}$$

$$\frac{\partial T}{\partial t} + u\frac{\partial T}{\partial x} + v\frac{\partial T}{\partial y} = \alpha_{nf}\left(\frac{\partial^2 T}{\partial x^2} + \frac{\partial^2 T}{\partial y^2}\right) \tag{4}$$

where $\alpha_{nf} = \frac{k_{nf}}{(\rho C_p)_{nf}}$ is the thermal diffusivity of the nanofluid.

The following dimensionless parameters can be used to convert the above equations into the dimensionless form as:

$$X = \frac{x}{H},\ Y = \frac{y}{H},\ U = \frac{u}{u_0},\ V = \frac{v}{u_0},\ P = \frac{p}{\rho_f u_0^2}$$
$$\theta = \frac{T - T_c}{T_h - T_c},\ \mathrm{Pr} = \frac{\nu_f}{\alpha_f},\ \mathrm{St} = \frac{fH}{u_0},\ \mathrm{Re} = \frac{u_0 H}{\nu_f},\ \tau = \frac{t u_0}{H} \quad (5)$$

The non-dimensional form of the governing equations can be obtained after substitution of the above non-dimensional variables as:

$$\frac{\partial U}{\partial X} + \frac{\partial V}{\partial Y} = 0 \quad (6)$$

$$\frac{\partial U}{\partial \tau} + U\frac{\partial U}{\partial X} + V\frac{\partial U}{\partial Y} = -\frac{\rho_f}{\rho_{nf}}\frac{\partial P}{\partial X} + \frac{\nu_{nf}}{\nu_f}\frac{1}{\mathrm{Re}}\left(\frac{\partial^2 U}{\partial X^2} + \frac{\partial^2 U}{\partial Y^2}\right) \quad (7)$$

$$\frac{\partial V}{\partial \tau} + U\frac{\partial V}{\partial X} + V\frac{\partial V}{\partial Y} = -\frac{\rho_f}{\rho_{nf}}\frac{\partial P}{\partial Y} + \frac{\nu_{nf}}{\nu_f}\frac{1}{\mathrm{Re}}\left(\frac{\partial^2 V}{\partial X^2} + \frac{\partial^2 V}{\partial Y^2}\right) \quad (8)$$

$$\frac{\partial \theta}{\partial \tau} + U\frac{\partial \theta}{\partial X} + V\frac{\partial \theta}{\partial Y} = \frac{1}{\mathrm{RePr}}\frac{k_{nf}}{k_f}\frac{(\rho c_p)_f}{(\rho c_p)_{nf}}\left(\frac{\partial^2 \theta}{\partial X^2} + \frac{\partial^2 \theta}{\partial Y^2}\right) \quad (9)$$

Boundary Conditions and Nusselt Number Calculation

For the backward-facing step geometry, boundary conditions in the non-dimensional form can be described as follows:

- At the channel inlet:
  $U = 1 + \sin(2\pi \mathrm{St}\tau),\ V = 0,\ \theta = 1$
- On the bottom wall downstream of the step:
  $U = V = 0,\ \theta = 1$
- For the remaining walls:
  $U = V = 0,\ \frac{\partial \theta}{\partial n} = 0$
- At the channel exit, outflow conditions were imposed:
  $\frac{\partial U}{\partial X} = 0,\ V = 0,\ \frac{\partial \theta}{\partial X} = 0$

The local Nusselt number for the hot wall is obtained as follows:

$$\mathrm{Nu}_{x,t} = -\frac{k_{nf}}{k_f}\left(\frac{\partial \theta}{\partial n}\right)_{n=0}, \quad (10)$$

where θ is the non-dimensional temperature and n represents the normal coordinate. The spatially-averaged Nusselt number and spatial-temporal averaged Nusselt number are calculated as follows:

$$\mathrm{Nu}_t = \frac{1}{H}\int_0^H \mathrm{Nu}_{x,t}dx,\ \ \mathrm{Nu}_m = \frac{1}{\tau}\frac{1}{H}\int_t^{\tau+t}\int_0^H \mathrm{Nu}_{x,t}dxdt. \quad (11)$$

Nanofluid Effective Thermophysical Properties

The effective thermophysical properties of the nanofluid are described as follows:

$$\rho_{nf} = (1-\phi)\rho_f + \phi\rho_p, \quad (12)$$

$$(\rho c_p)_{nf} = (1-\phi)(\rho c_p)_f + \phi(\rho c_p)_p, \quad (13)$$

$$(\rho\beta)_{nf} = (1-\phi)(\rho\beta)_f + \phi(\rho\beta)_p. \quad (14)$$

The effective thermal conductivity of the nanofluid includes the effect of Brownian motion, and it is given as [22]:

$$k_{nf} = k_{st} + k_{Brownian} \tag{15}$$

where k_{st} is defined by [23]:

$$k_{st} = k_f \left[\frac{(k_p + 2k_f) - 2\phi(k_f - k_p)}{(k_p + 2k_f) + \phi(k_f - k_p)} \right] \tag{16}$$

while $k_{Brownian}$ is given as:

$$k_{Brownian} = 5 \times 10^4 \times 1.9526 \times (100\phi)^{-1.4594} \phi \rho_f c_{p,f} \sqrt{\frac{\kappa_b T}{\rho_p d_p}} f'(T, \phi) \tag{17}$$

where the function f' is given in [22], and it is valid for the solid volume fraction of nanoparticle up to $\phi \leq 4\%$ and temperature values between 300 K $< T <$ 325 K.

The effective viscosity model of the nanofluid was given in [24]:

$$\mu_{nf} = \mu_f \frac{1}{\left(1 - 34.87 \left(\frac{d_p}{d_f}\right)^{-0.3} \phi^{1.03}\right)} \tag{18}$$

with the average particle size of the fluid:

$$d_f = \left(\frac{6M}{N\pi\rho_f}\right)^{1/3}, \tag{19}$$

where M and N are the molecular weight and Avogadro number.

The above correlation is valid for a nanoparticle volume fraction up to $\phi \leq 7.1\%$ and temperatures between 293 K $< T <$ 323 K [24].

The particle shape effects on the effective thermal conductivity and viscosity of the nanofluid are described as follows [19]:

$$k_{nf} = k_f (1 + C_k \phi), \tag{20}$$

$$\mu_{nf} = \mu_f \left(1 + A_1 \phi + A_2 \phi^2\right) \tag{21}$$

where the constant coefficients for different nanoparticle shapes in the above given expressions are defined as in Table 2 [19]. In this study, the Newtonian behavior of the nanofluid was assumed even with the highest solid volume fraction of $\phi = 4\%$ considered in this work. In the numerical study of [19], the nanofluid with various nanoparticle shapes was considered up to a solid volume fraction of $\phi = 4\%$, which was used as a reference in this study for the effect of particle shape on the thermal conductivity and viscosity for the SiO_2-water nanofluid.

Table 2. Constant coefficients defined in Equation (20) and Equation (21) for the effective viscosity and thermal conductivity of the nanofluid for various nanoparticle shapes [19].

Nanoparticle Shape	C_k	A_1	A_2
cylindrical	3.95	13.5	904.4
bricks	3.37	1.9	471.4
blades	2.74	14.6	123.3

3. Solution Methodology

Numerical simulations are performed by using the finite volume method. For velocity-pressure coupling, the SIMPLE (Semi-Implicit Method for Pressure-Linked Equations) algorithm of [25] was used, and to discretize the convective terms in the momentum and energy equations, the QUICK (Quadratic Upstream Interpolation for Convective Kinematics) scheme [26] was utilized. A set of algebraic equations was obtained, and the equation for a fluid variable ϕ at the node point p, which is in the neighborhood of the relevant nodes (subscript n), can be written as [27]:

$$a_p\phi_p = \sum a_n\phi_n + b \tag{22}$$

with b being a constant. The Gauss–Seidel point-by-point iterative method and algebraic multigrid method were utilized for the solution of the resulting system of algebraic equations. The residual, which is normalized, can be defined as:

$$R^{\phi} = \frac{\sum_{allcells} |a_p\phi_p - a_n\phi_n - b|}{\sum_{allcells} |a_p\phi_p|}. \tag{23}$$

The iterative solution is assumed to be in progress when the residuals for all dependent variables become less than 10^{-5}. The under-relaxation parameter for pressure correction was set to 0.3, while for u, v and T, a value of 0.6 was chosen. Finer mesh resolutions were used near the wall and step, especially for the region where flow separation and reattachment occurs. Various grid sizes with different numbers of elements were used to obtain a mesh-independent solution. Table 3 shows the grid independence result for cylindrical particles with two values of nanoparticle volume fraction. Grid G4 with 9848 elements is used in the subsequent computations.

For the unsteady computations, the second order implicit formulation with a time step size of Δt was used. Time step size of 1/50th of the period of the oscillation $\Delta t = \tau_p/50$ was used to ensure the time step size independence of the solution. Numerical code is validated with the results of Khandelwal et al. [28], where fluid flow in a T-channel was numerically examined with the finite volume-based method. Table 4 shows the comparison results of the recirculation lengths at different Reynolds numbers.

Table 3. Grid independence test with spherical particles at two different solid particle volume fractions.

Grid Name	Number of Elements	Nu_m ($\phi = 0\%$)	Nu_m ($\phi = 4\%$)
G1	632	0.965	1.345
G2	1430	1.243	1.594
G3	6240	1.436	1.795
G4	9848	1.455	1.836
G5	67,256	1.467	1.865

Table 4. Comparison of the recirculation lengths with the results of Khandelwal et al. [28].

Re	L_R/D (Khandelwal et al. [28])	L_R/D (Present Solver)	Difference (%)
100	2.73	2.64	−3.29
150	3.39	3.36	−0.88
200	3.99	3.96	−0.75

4. Results and Discussion

The main aim of the present study was to examine the nanoparticle shape effects on the fluid flow and heat transfer characteristics in a laminar pulsating nanofluid flow over a backward-facing step geometry. The Reynolds number, amplitude of flow pulsation and expansion ratio of the channel were fixed to 200, 0.6 and 2, respectively. The frequency of the pulsating flow (Strouhal number between 0.1 and 2), nanoparticle volume fraction (between 0 and 0.04) and nanoparticle shape (spherical, blade and cylindrical) were changed during the simulation.

The effects of the nanoparticle shape and solid volume fraction on the reattachment length are shown in Figure 2. For the nanofluid with the cylindrically-shaped particles, higher viscosity resulted in a lower Reynolds number, and therefore, the reattachment length was lower. Steep temperature gradients were obtained near the reattachment point, and heat transfer was locally higher for those locations, which were also shown in the previous studies [6,7]. The discrepancy between different solid particle shapes was higher for the higher particle volume fraction. The effects of the particle shape on the variation of the x-component velocity along the y-axis for two different fixed locations at $x = H$ and $x = 5H$ are shown in Figure 3. For location $x = H$, from $y = 0.13H$ until the upper wall, the velocity was higher for spherical particles. Downstream of the step at $x = 5H$, the velocity was higher for cylindrically- and blade-shaped particles compared to spherical ones near the upper and lower channel walls. The effects of the solid volume fraction for the cylindrically-shaped particles on the variation of the x-velocity for the same locations as in Figure 3 are demonstrated in Figure 4. In the recirculation region and near the upper wall (from $y = 1.2H$ to $y = 2H$), increasing the particle volume fraction reduced the fluid velocity (Figure 4). Far away from the step, the velocity was higher for a higher particle volume fraction near the upper and bottom walls of the channel.

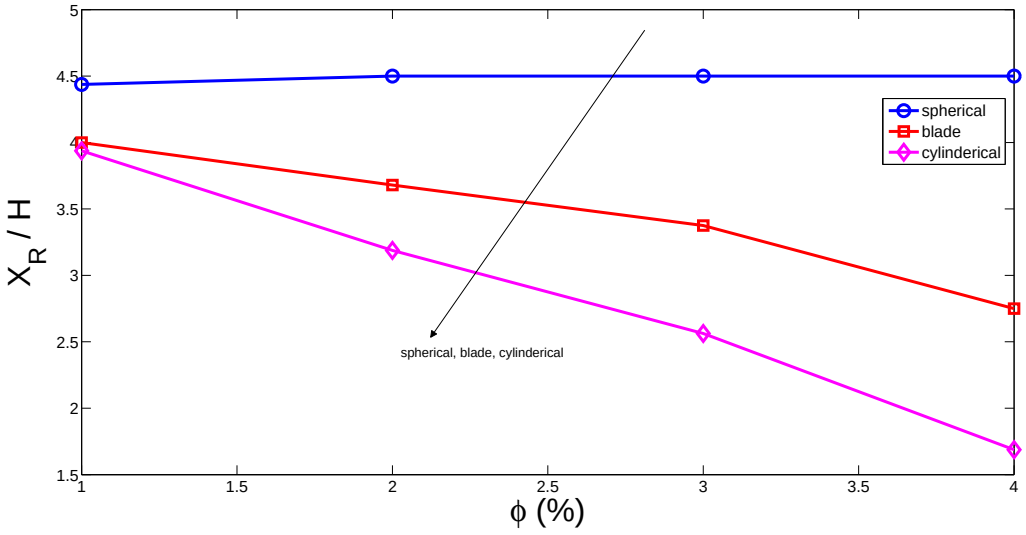

Figure 2. Particle size effect on the reattachment length for various nanoparticle volume fractions.

Local variation of the Nusselt number for hot wall with various particle volume fractions and various particle shapes is shown in Figure 5. For the spherically-shaped particles, enhancing the solid particle volume fraction resulted in higher values of local Nusselt number, which was due to the thermal conductivity enhancement and better thermal transport properties of the nanofluid. The shift in the peak Nusselt number toward the step was seen for higher ϕ values, which was due to the reduction of the reattachment length for higher particle volume fractions. The cylinder-shaped particle showed the highest local heat transfer enhancement, and the peak value was closer to the step, which

was due to the reduction of the reattachment length (Figure 5). The behavior of the cylindrical particle shape on the heat transfer enhancement shows similar trends as examined in the studies [17,29].

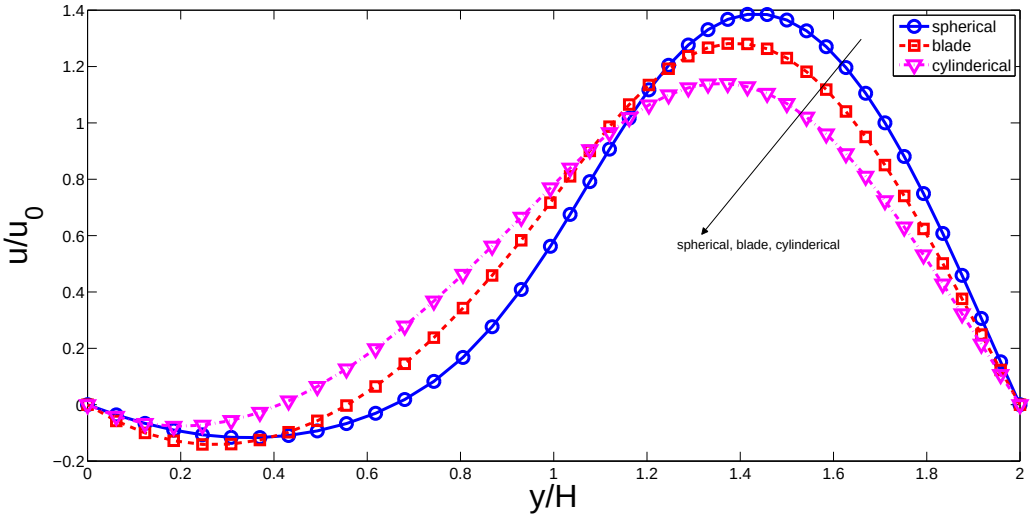

(**a**) $x = H$

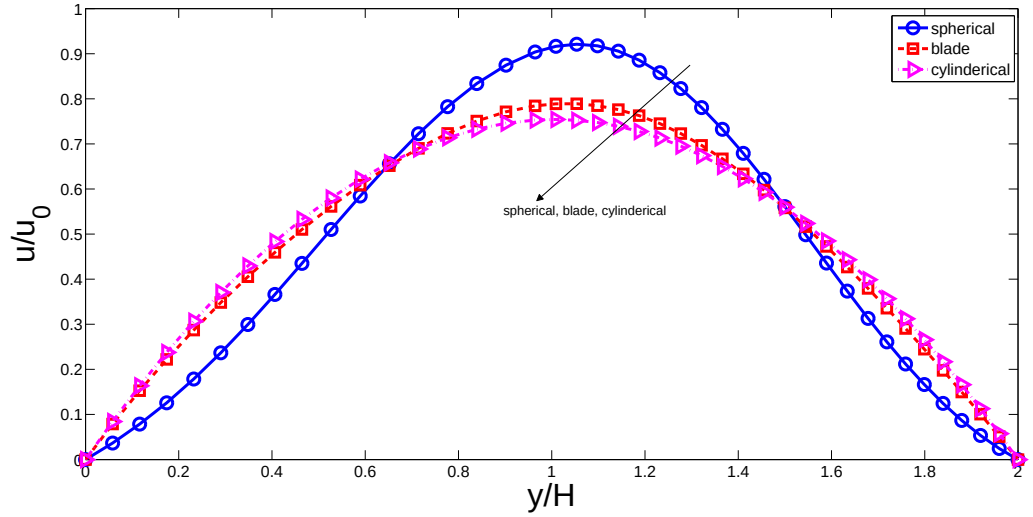

(**b**) $x = 5H$

Figure 3. Variation of the x component velocity along the y direction for various particle shapes with $\phi = 0.02$.

The distribution of streamlines and isotherms for different time instances within a period ($t_1 = t_{last}$, $t_2 = t_{last} - 10\Delta t$, $t_3 = t_{last} - 20\Delta t$, $t_4 = t_{last} - 40\Delta t$ with t_{last} as the last time step) when the system reaches steady oscillation state is shown in Figures 6 and 7 for the nanofluid with spherical and cylindrical nanoparticles. A recirculation region was formed behind the step, and its size changed for different time instances within a period of oscillation. Near the upper part of the channel, a secondary recirculation zone was formed, which was also shown in the previous studies for pulsating flow over a backward-facing step geometry for a nanofluid with a spherical nanoparticle. The vortex size behind the step was smaller for the nanofluid with a cylindrically-shaped particle, and its size changed for different time steps. Steep temperature gradients were seen in the locations near the reattachment point.

For the hot wall downstream of the step, the temperature gradients became steeper with cylindrical particle shapes, which have higher thermal conductivity compared to the other particle shapes. These locally effective heat transfer locations changed for various time instances.

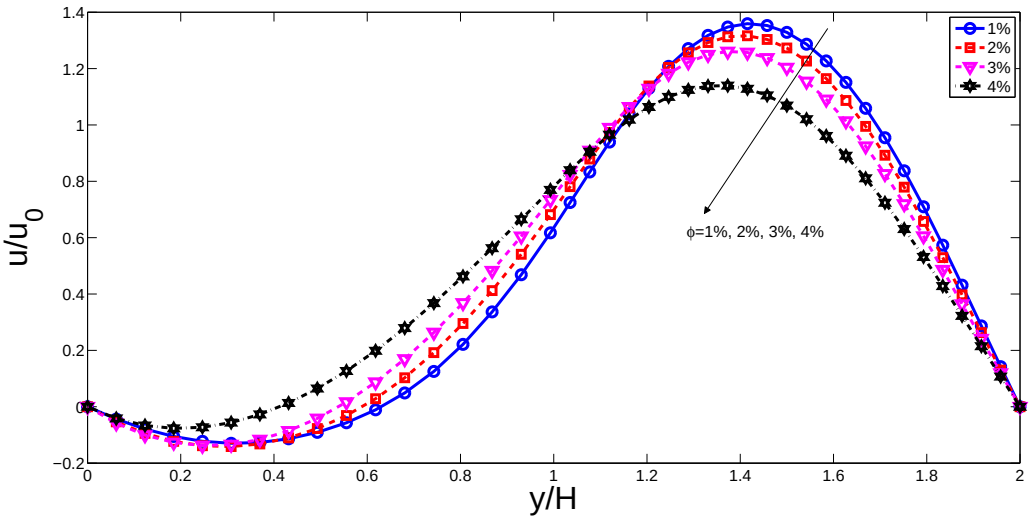

(**a**) $x = H$

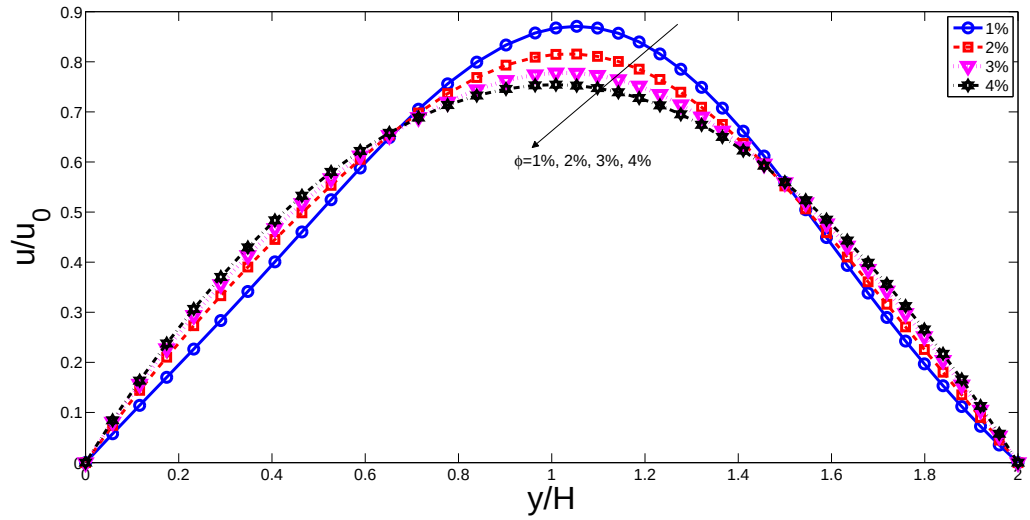

(**b**) $x = 5H$

Figure 4. Variation of the x component velocity along the y direction for various nanoparticle volume fractions with cylindrically-shape particles.

The spatially-averaged Nusselt number for the hot wall of the backward-facing step geometry for various particle shapes and Strouhal numbers are shown in Figure 8. The number of cycles to reach the steady oscillation state was higher for higher Strouhal numbers. This is due to the flow adaptation time becoming significant for higher frequencies, which were also shown in the previous studies for pulsating flow over a backward-facing step [30,31]. Nanoparticle addition enhanced the spatially-averaged heat transfer, which was due to the thermal conductivity enhancement of the nanofluid. Among different nanoparticle shapes, nanofluids with blade-shaped particles have the lowest heat transfer values. The spatial-temporal average Nusselt number versus solid particle

volume fractions are shown in Figure 9 for various particle shapes at two different Strouhal numbers. The spatially-averaged Nusselt number for various particle shapes are also included in the plots. The discrepancy between the average Nusselt number for various particle shapes was higher for a high particle concentration, as can be noticed from the thermal conductivity expression, which had a linear dependence on the particle volume fraction for cylindrically- and blade-shaped particles. As the value of the Strouhal number enhanced, the average Nusselt number values in the steady and pulsating flow conditions became closer, especially for the lower values of particle volume fractions.

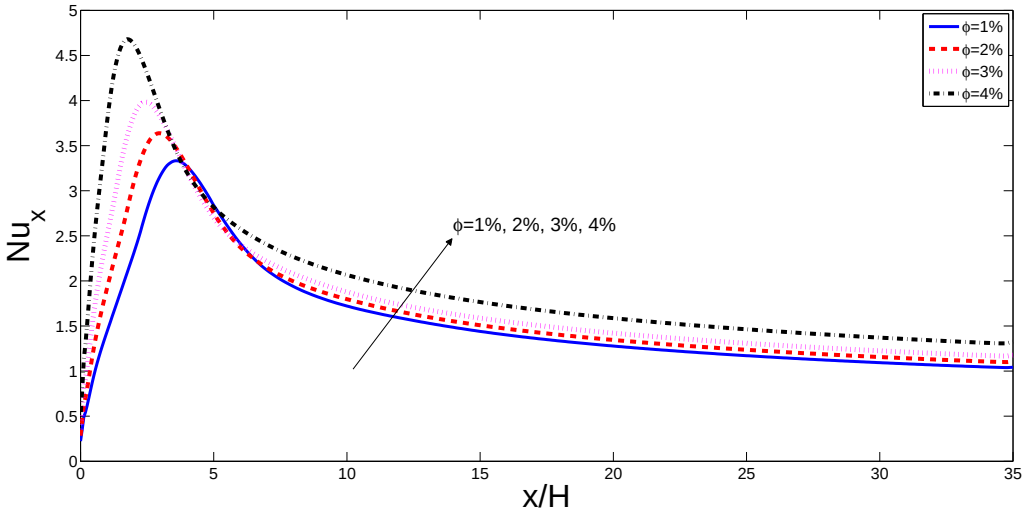

(**a**) spherical shape

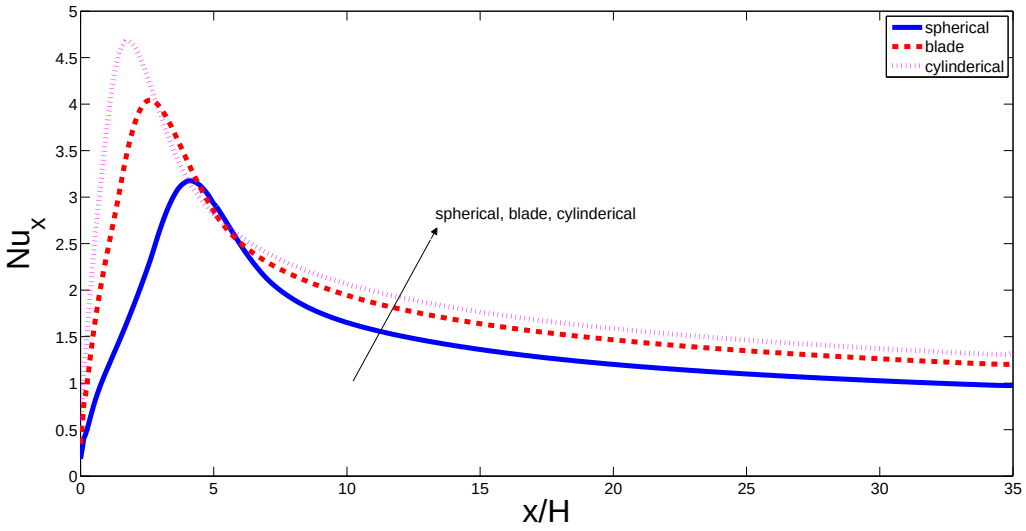

(**b**) $\phi = 0.02$

Figure 5. Effects of the particle shape and volume fraction on the local Nusselt number distribution along the hot bottom wall downstream of the step.

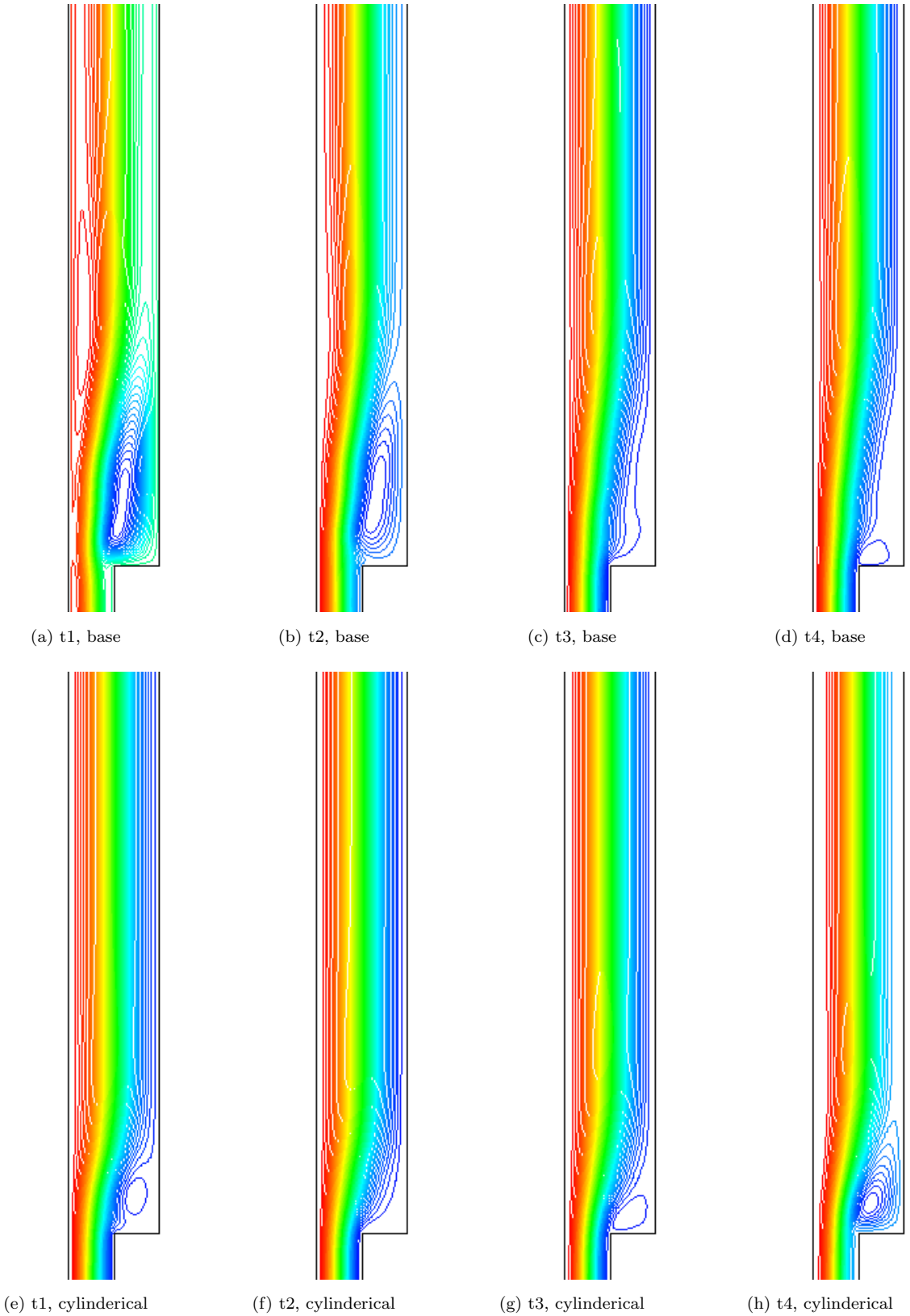

(a) t1, base (b) t2, base (c) t3, base (d) t4, base

(e) t1, cylinderical (f) t2, cylinderical (g) t3, cylinderical (h) t4, cylinderical

Figure 6. Variation of streamlines for several time instances within a period for the base fluid and for the nanofluid with cylindrical nanoparticles.

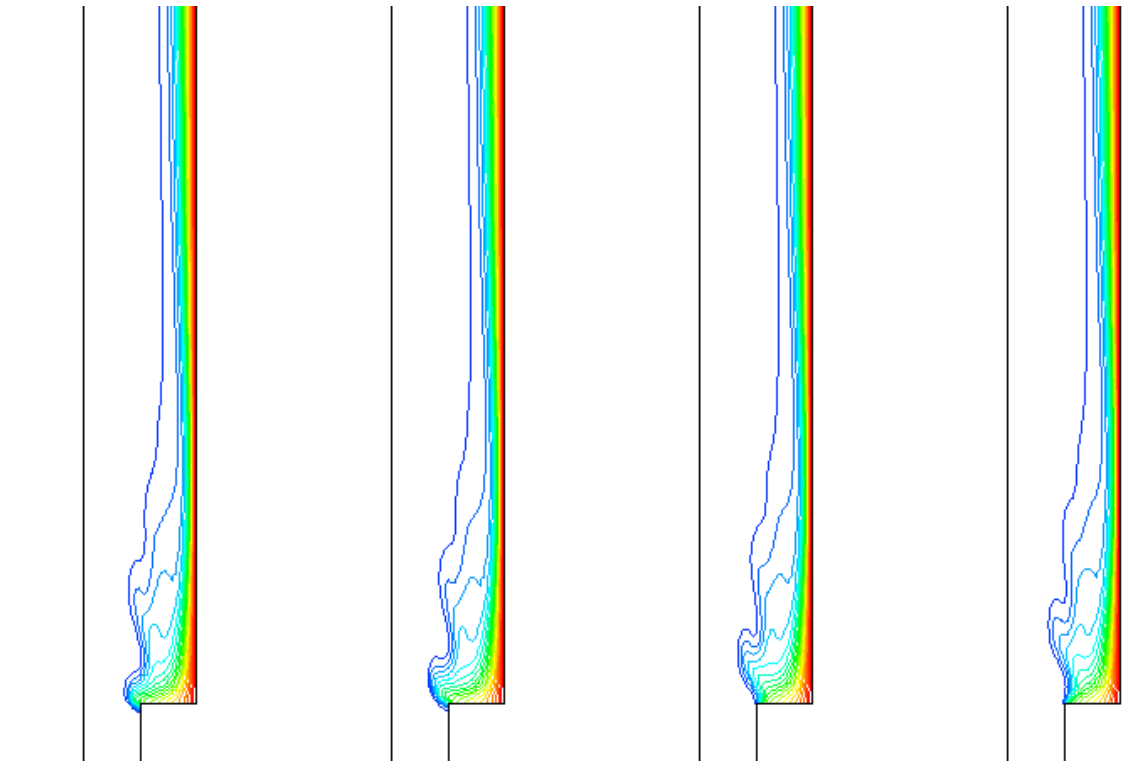

(a) t1, base (b) t2, base (c) t3, base (d) t4, base

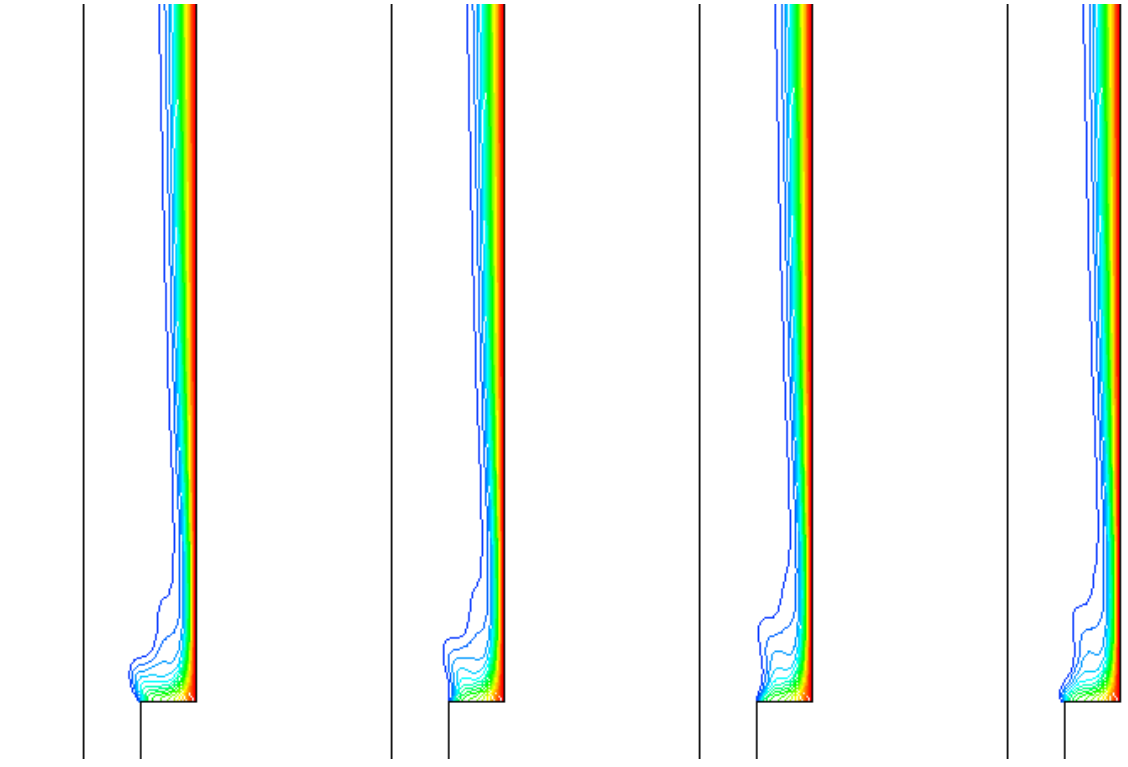

(e) t1, cylinderical (f) t2, cylinderical (g) t3, cylinderical (h) t4, cylinderical

Figure 7. Isotherm distributions for several time instances within a period for the base fluid and for the nanofluid with cylindrical nanoparticles.

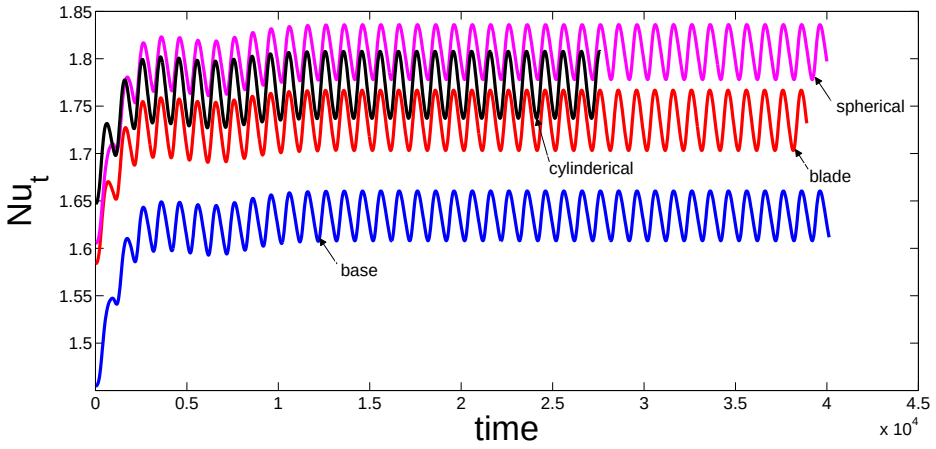

(**a**) St=0.1

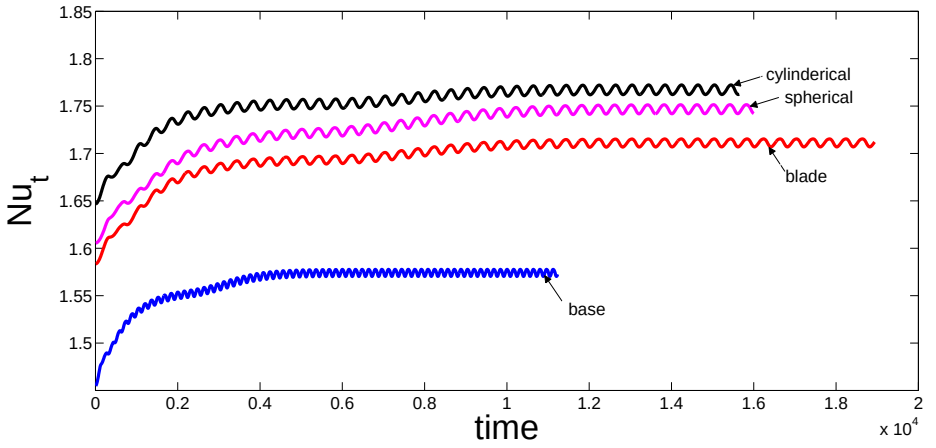

(**b**) St=0.25

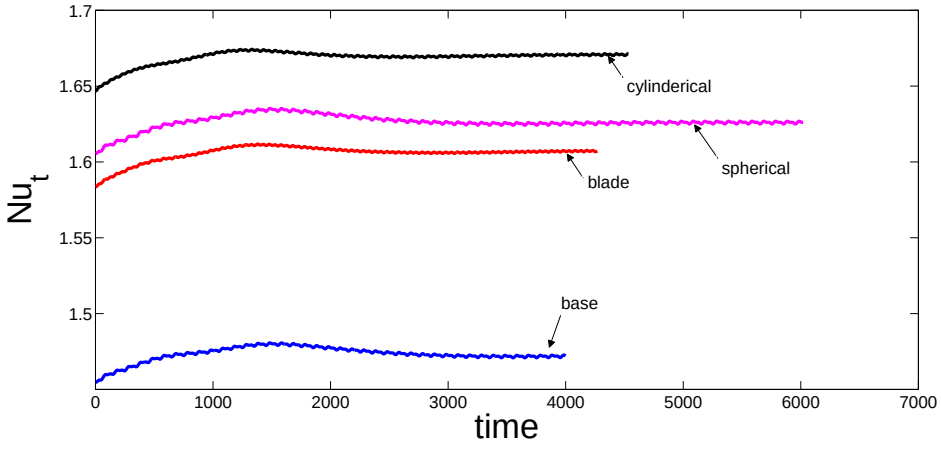

(**c**) St=1

Figure 8. Effects of particle shape on the spatially-average Nusselt number along the hot wall for various pulsating frequencies.

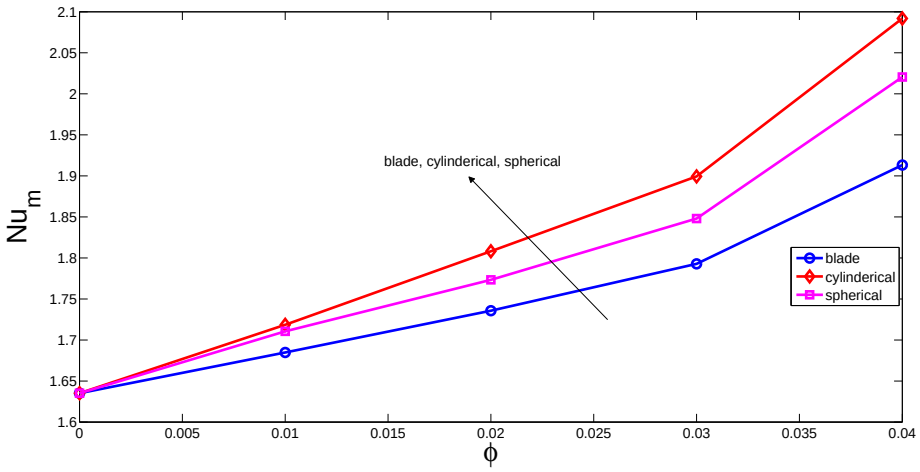

(**a**) St=0.1

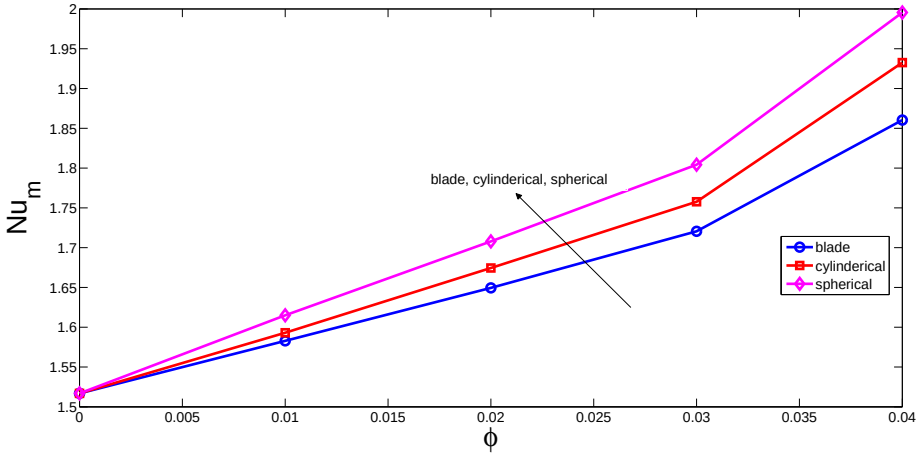

(**b**) St=0.5

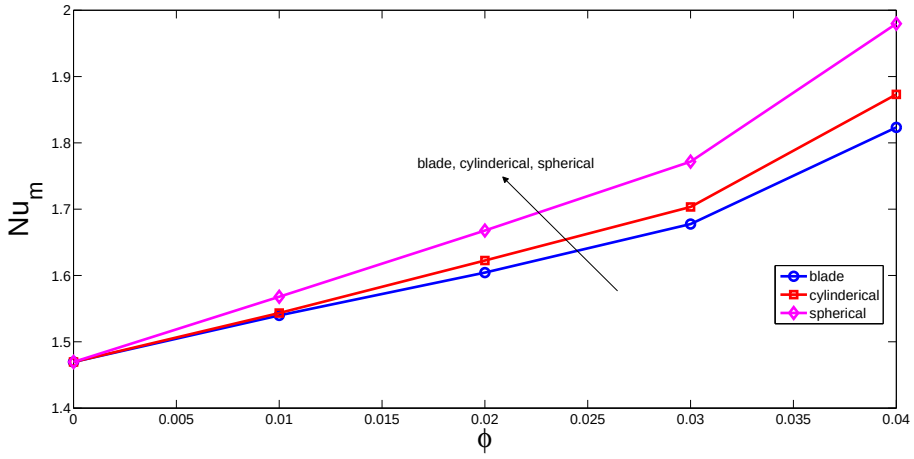

(**c**) St=2

Figure 9. Average Nusselt numbers versus solid particle volume fractions for various pulsating frequencies and nanoparticle shapes.

The effects of pulsation frequency in terms of Strouhal number on the spatial and spatio-temporally-averaged Nusselt number, which are defined by Equations (10) and (11), are demonstrated in Figures 10–12 for various particle shapes. As compared to the base fluid, the inclusion of the nanoparticles resulted in different oscillation characteristics for the Nusselt numbers among different Strouhal numbers. The highest value of the spatially-averaged Nusselt number was seen for a Strouhal number of 0.1, and for cylindrically- and blade-shaped particles, the discrepancy between the Nusselt number values at St = 0.1 and St = 0.25 became less. As is shown in Figure 12, the spatially-averaged Nusselt number reduces with the Strouhal number (a resonant-type behavior can also be seen if lower Strouhal number values were also considered). A higher solid particle volume fraction enhanced the spatio-temporally-averaged Nusselt number, both in pulsating flow and steady flow configurations. The discrepancy between the Nusselt number in pulsating flow and the steady case reduced for higher values of the Strouhal number. For the lowest Strouhal number of interest, the average Nusselt number enhanced by about 27.95%, whereas in the steady case, it was increased by about 12.37% for the highest particle volume fraction ($\phi = 0.04$) compared to the base fluid. It is seen that the dynamics of fluid in pulsating flow conditions contributed to more heat transfer enhancement when nanoparticles were included in the base fluid. Table 5 shows the Heat Transfer Enhancement (HTE) results for various particle shapes in steady and pulsating flow configurations at the highest solid particle volume fraction compared to the base fluid. It is seen that using the spherical particles was advantageous for heat transfer enhancement in pulsating flow as compared to blade- and cylindrically-shaped particles. The particle shape effect influence on the convective heat transfer enhancement feature was different in pulsating flow as compared to steady flow, which reveals that the dynamics of the flow features were highly affected by the variation of the thermophysical properties along with the flow conditions and geometry of the problem.

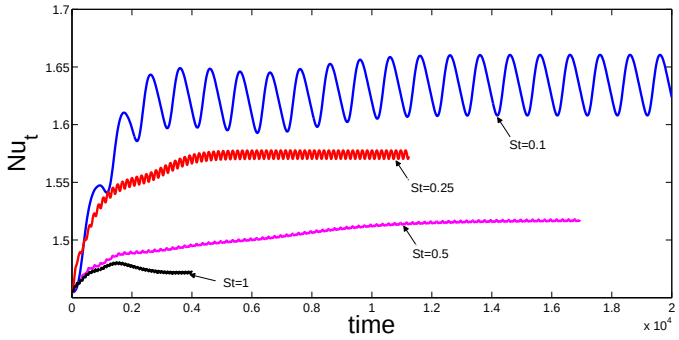

(**a**) base fluid

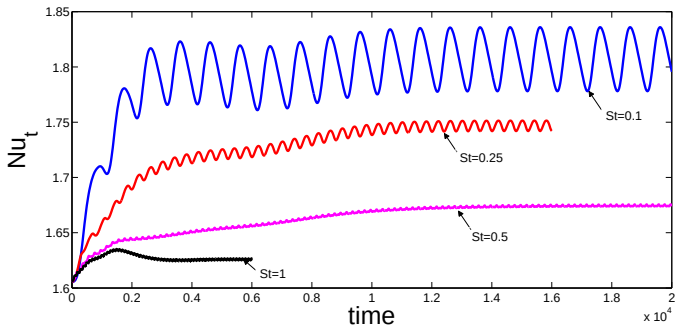

(**b**) spherical

Figure 10. The effects of the Strouhal number on the spatially-averaged Nusselt number along the hot wall for water and the spherical particle shape with $\phi = 0.02$.

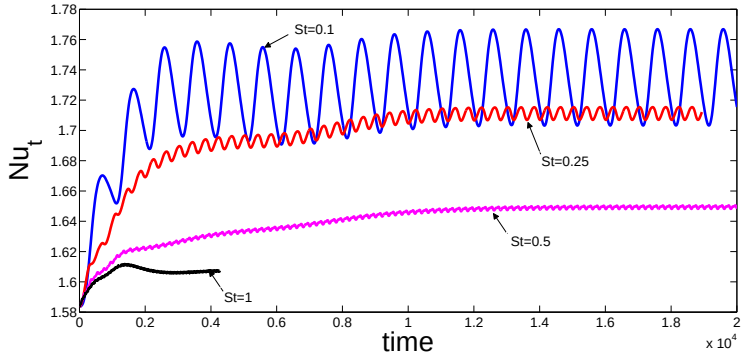

(**a**) blade

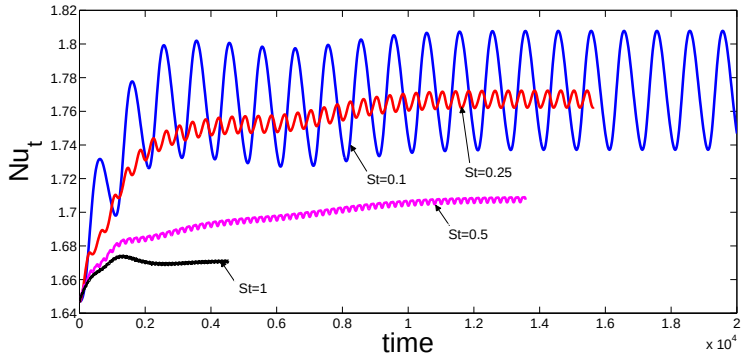

(**b**) cylindrical

Figure 11. The effects of the Strouhal number on the spatially-averaged Nusselt number along the hot wall for the blade and cylindrical particle shapes with $\phi = 0.02$.

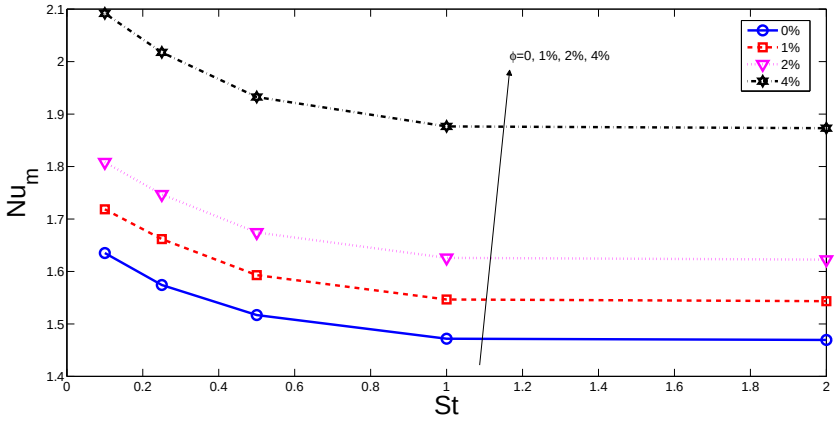

Figure 12. The average Nusselt number versus the Strouhal number for different nanoparticle volume fractions with spherically-shaped particles.

Table 5. Spatial-temporal average Nusselt number for various particle shapes at a Strouhal number of 0.1 and $\phi = 0.04$. HTE, Heat Transfer Enhancement.

Particle Type	Nu_s (Steady)	Nu_m (Pulsating)	HTE in Steady (%)	HTE in Pulsating (%)
Spherical	1.635	2.092	12.37	27.95
Blade	1.836	1.950	26.185	19.26
Cylindrical	1.895	1.953	30.24	19.44

5. Conclusions

Numerical simulation of the forced convection of pulsating nanofluid flow over a backward-facing step geometry with various nanoparticle shapes was performed. It was observed that the recirculation region behind the step is affected by the presence of the different nanoparticle shapes. Reattachment length and the x-velocity component were found to be very sensitive to the particle shape. In all cases, the average Nusselt number was a decreasing function of the Strouhal number and an increasing function of the solid volume fraction of nanoparticles. Heat transfer enhancement in pulsating flow is higher for the nanofluid with a spherical shape, and up to a 27.95% average heat transfer is obtained for a volume fraction of 4%. However, for the steady configuration, it is advantageous to use cylindrically-shaped nanoparticles, and up to a 30.24% heat transfer enhancement is achieved for the highest solid particle volume fraction.

Author Contributions: F.S. performed the numerical simulations and wrote some sections of the manuscript. A.J.C. prepared some other sections of the paper and analyzed the results. All of the authors contributed equally to reviewing and revising the manuscript.

Funding: This research received no external funding.

Conflicts of Interest: The authors declare no conflict of interest.

Abbreviations

A	amplitude of pulsation
f	frequency of pulsation
h	local heat transfer coefficient
k	thermal conductivity
H	step size
n	unit normal vector
Nu_x	local Nusselt number
Nu_m	averaged Nusselt number
p	pressure
Pr	Prandtl number
Re	Reynolds number
St	Strouhal number
T	temperature
t	time
u, v	x-y velocity components
x, y	Cartesian coordinates

Greek Characters

α	thermal diffusivity
β	expansion coefficient
ϕ	solid volume fraction
ν	kinematic viscosity
θ	non-dimensional temperature
ρ	density of the fluid

Subscripts

c	cold
h	hot
m	average
nf	nanofluid
p	solid particle
st	static

References

1. Armaly, B.F.; Durst, F.; Pereier, J.C.F.; Schonung, B. Experimental and theoretical investigation of backward-facing step flow. *J. Fluid Mech.* **1983**, *127*, 473–496. [CrossRef]
2. Sherry, M.; LoJacono, D.; Sheridan, J. An experimental investigation of the recirculation zone formed downstream of a forward facing step. *J. Wind Eng. Ind. Aerodyn.* **2010**, *98*, 888–894. [CrossRef]
3. Abu-Mulaweh, H. Turbulent mixed convection flow over a forward-facing step—The effect of step heights. *Int. J. Therm. Sci.* **2005**, *44*, 155–162. [CrossRef]
4. Barkley, D.; Gomes, M.G.M.; Henderson, R.D. Three-dimensional instability in flow over a backward-facing step. *J. Fluid Mech.* **2002**, *473*, 167–190. [CrossRef]
5. Iwai, H.; Nakabe, K.; Suzuki, K. Flow and heat transfer characteristics of backward-facing step laminar flow in a rectangular duct. *Int. J. Heat Mass Transf.* **2000**, *43*, 457–471. [CrossRef]
6. Kumar, A.; Dhiman, A.K. Effect of a circular cylinder on separated forced convection at a backward-facing step. *Int. J. Therm. Sci.* **2012**, *52*, 176–185. [CrossRef]
7. Selimefendigil, F.; Oztop, H.F. Effect of a rotating cylinder in forced convection of ferrofluid over a backward-facing step. *Int. J. Heat Mass Transf.* **2014**, *71*, 142–148. [CrossRef]
8. Selimefendigil, F.; Oztop, H.F. Laminar Convective Nanofluid Flow over a Backward-Facing Step with an Elastic Bottom Wall. *J. Thermal Sci. Eng. Appl.* **2018**, *10*, 041003. [CrossRef]
9. Selimefendigil, F.; Oztop, H.F. Influence of inclination angle of magnetic field on mixed convection of nanofluid flow over a backward-facing step and entropy generation. *Adv. Powder Technol.* **2015**, *26*, 1663–1675. [CrossRef]
10. Jin, D.; Lee, Y.; Lee, D. Effects of the pulsating flow agitation on the heat transfer in a triangular grooved channel. *Int. J. Heat Mass Transf.* **2007**, *50*, 3062–3071. [CrossRef]
11. Faghri, M.; Javdani, K.; Faghri, A. Heat transfer with laminar pulsating flow in a pipe. *Lett. Heat Mass Transf.* **1979**, *6*, 259–270. [CrossRef]
12. Cho, H.; Hyun, J. Numerical solutions of pulsating flow and heat transfer characteristics in a pipe. *Int. J. Heat Fluid Flow* **1990**, *11*, 321–330. [CrossRef]
13. Nield, D.; Kuznetsov, A. Forced convection with laminar pulsating flow in a channel or tube. *Int. J. Therm. Sci.* **2007**, *46*, 551–560. [CrossRef]
14. Abu-Nada, E. Application of nanofluids for heat transfer enhancement of separated flows encountered in a backward-facing step. *Int. J. Heat Fluid Flow* **2008**, *29*, 242–249. [CrossRef]
15. Togun, H.; Ahmadi, G.; Abdulrazzaq, T.; Shkarah, A.J.; Kazi, S.; Badarudin, A.; Safaei, M. Thermal performance of nanofluid in ducts with double forward-facing steps. *J. Taiwan Inst. Chem. Eng.* **2015**, *47*, 28–42. [CrossRef]
16. Selimefendigil, F.; Oztop, H.F. Identification of forced convection in pulsating flow at a backward facing step with a stationary cylinder subjected to nanofluid. *Int. Commun. Heat Mass Transf.* **2013**, *45*, 111–121. [CrossRef]
17. Selimefendigil, F.; Oztop, H.F.; Abu-Hamdeh, N. Mixed convection due to rotating cylinder in an internally heated and flexible walled cavity filled with SiO_2–Water nanofluids: Effect of nanoparticle shape. *Int. Commun. Heat Mass Transf.* **2016**, *71*, 9–19. [CrossRef]
18. Selimefendigil, F.; Oztop, H.F. Mixed convection in a two-sided elastic walled and SiO2 nanofluid filled cavity with internal heat generation: Effects of inner rotating cylinder and nanoparticle's shape. *J. Mol. Liq.* **2015**, *212*, 509–516. [CrossRef]
19. Vanaki, S.; Mohammed, H.; Abdollahi, A.; Wahid, M.A. Effect of nanoparticle shapes on the heat transfer enhancement in awavy channel with different phase shifts. *J. Mol. Liq.* **2014**, *196*, 32–42. [CrossRef]
20. Jeong, J.; Li, C.; Kwon, Y.; Lee, J.; Kim, S.H.; Yun, R. Particle shape effect on the viscosity and thermal conductivity of ZnO nanofluids. *Int. J. Refrig.* **2013**, *36*, 2233–2241. [CrossRef]
21. Murshed, S.; Leong, K.; Yang, C. Enhanced thermal conductivity of TiO_2—Water based nanofluids. *Int. J. Therm. Sci.* **2005**, *44*, 367–373. [CrossRef]
22. Vajjha, R.; Das, D.; Kulkarni, D. Development of new correlations for convective heat transfer and friction factor in turbulent regime for nanofluids. *Int. J. Heat Mass Transf.* **2010**, *53*, 4607–4618. [CrossRef]
23. Maxwell, J. *A Treatise on Electricity and Magnetism*; Oxford University Press: Oxford, UK, 1873.
24. Corcione, M. Heat transfer features of buoyancy-driven nanofluids inside rectangular enclosures differentially heated at the sidewalls. *Int. J. Therm. Sci.* **2010**, *49*, 1536–1546. [CrossRef]

25. Patankar, S.V. *Numerical Heat Transfer and Fluid Flow*; McGraw Hill: New York, NY, USA, 1980.
26. Leonard, B.P. A stable and accurate convective modelling procedure based on quadratic upstream interpolation. *Comput. Methods Appl. Mech. Eng.* **1979**, *19*, 59–98. [CrossRef]
27. Versteeg, H.; Malalasekera, W. *An Introduction to Computational Fluid Dynamics. The Finite Volume Method*; Longman: Harlow, UK, 1995.
28. Khandelwal, V.; Dhiman, A.; Baranyi, L. Laminar flow of non-Newtonian shear-thinning fluids in a T-channel. *Comput. Fluids* **2015**, *108*, 79–91. [CrossRef]
29. Selimefendigil, F.; Oztop, H.F. Effects of Nanoparticle Shape on Slot-Jet Impingement Cooling of a Corrugated Surface With Nanofluids. *J. Therm. Sci. Eng. Appl.* **2017**, *9*, 021016. [CrossRef]
30. Selimefendigil, F.; Oztop, H.F. Control of Laminar Pulsating Flow and Heat Transfer in Backward-Facing Step by Using a Square Obstacle. *J. Heat Transf.* **2014**, *136*, 081701. [CrossRef]
31. Selimefendigil, F.; Oztop, H.F. Numerical analysis of laminar pulsating flow at a backward-facing step with an upper wall mounted adiabatic thin fin. *Comput. Fluids* **2013**, *88*, 93–107. [CrossRef]